Partanen, Mikko; Tulkki, Jukka

Angular momentum dynamics of light-driven mass density waves in thin film structures

Published in:
Complex Light and Optical Forces XIII

DOI:
10.1117/12.2505844

Published: 01/01/2019

Document Version
Publisher's PDF, also known as Version of record

Please cite the original version:
Partanen, M., & Tulkki, J. (2019). Angular momentum dynamics of light-driven mass density waves in thin film structures. In E. J. Galvez, D. L. Andrews, & J. Gluckstad (Eds.), *Complex Light and Optical Forces XIII* (pp. 1-10). Article 109350B (Proceedings of SPIE; Vol. 10935). SPIE. https://doi.org/10.1117/12.2505844

PROCEEDINGS OF SPIE

SPIEDigitalLibrary.org/conference-proceedings-of-spie

Angular momentum dynamics of light-driven mass density waves in thin film structures

Mikko Partanen, Jukka Tulkki

Mikko Partanen, Jukka Tulkki, "Angular momentum dynamics of light-driven mass density waves in thin film structures," Proc. SPIE 10935, Complex Light and Optical Forces XIII, 109350B (1 March 2019); doi: 10.1117/12.2505844

SPIE.

Event: SPIE OPTO, 2019, San Francisco, California, United States

Angular momentum dynamics of light-driven mass density waves in thin film structures

Mikko Partanen and Jukka Tulkki

Engineered Nanosystems Group, School of Science
Aalto University, P.O. Box 12200, 00076 Aalto, Finland

ABSTRACT

We have recently developed the mass-polariton (MP) theory of light to describe propagation of light in dielectric materials [Phys. Rev. A 95, 063850 (2017)]. The MP theory considers a light wave simultaneously with the dynamics of the medium atoms driven by optoelastic forces between the field-induced dipoles and the electromagnetic field. The MP theory combines the well-known optical forces with the Newtonian dynamics of the medium. Therefore, it can be applied to any inhomogeneous, dispersive, and lossy materials. One of the key observations of the MP theory of light is that a light pulse propagating in a nondispersive dielectric transfers an increased atomic density such that the total transferred mass is equal to $\delta M = (n^2 - 1)E/c^2$, where n is the refractive index and E is the electromagnetic energy of the pulse. This mass is transferred by an atomic mass density wave (MDW) where the atoms are spaced more densely inside the light pulse as a result of the optical force. Another key observation is that, in common semiconductors, most of the linear and angular momenta of light is transferred by the semiconductor atoms in the MDW moving under the influence of the optical force. In this work, we use the electric and magnetic fields of selected Laguerre-Gaussian mode beams to calculate the optical force density, which is used in the optoelastic continuum dynamics to simulate the dynamics of medium atoms in edge-supported free-standing thin film structures. The goal of our work is to find out how the different force components related to the reflection, transmission, absorption, and the atomic MDW bend and twist the film. The simulations also aim at optimizing experimental studies of the atomic dynamics in the thin film and to relating the measurements to the properties of incoming light.

Keywords: mass-polariton, mass density wave, optical shock wave, electrodynamics, optomechanics

1. INTRODUCTION

Recently, the momentum and angular momentum of light have been investigated in vacuum,[1,2] in photonic materials,[3–6] in the near-field regime,[7–10] and also in the quantum domain.[11,12] The small elastic waves of atoms related to the momentum transfer by the reflection of light from a mirror have also been experimentally measured.[13,14] Despite the long history of the optics of thin film structures, the coupled space and time dependent dynamics of the field and the medium atoms in thin films and its relation to the linear and angular momenta of light have not been investigated in detail. Only a few related, but not very detailed, studies exist.[15,16] Recently, the coupled mass-polariton (MP) description of the field and medium dynamics has been investigated in the case of homogeneous dielectric materials[17–20] and optical waveguides,[21] but detailed studies of the effects arising from the coupled field-medium dynamics do not exist for edge-supported free-standing thin film structures. The works on the coupled dynamics of the field and the medium atoms show that light is associated with an atomic mass density wave (MDW) that is both necessary for the fulfillment of Newton's first law and it also carries a major part of the total linear and angular momenta of light in many common dielectrics.

The MP theory of light combines Maxwell's equations of the field with the Newtonian mechanics of the medium.[17] The related optoelastic continuum dynamics (OCD) simulations allow detailed studies of the coupled dynamics of the field and the medium. In the present work, we study the coupled field-medium dynamics and related effects in thin film structures. We first review the foundations of the MP theory and its numerical implementation using the OCD model. We also perform OCD simulations of the field-medium dynamics in the case of selected continuous wave (cw) Laguerre-Gaussian mode light beams to find out how the different force components related to the reflection, transmission, absorption, and the atomic MDW bend the low-loss and lossy thin film structures. The simulations also aim at optimizing experimental studies of the atomic dynamics in the

Complex Light and Optical Forces XIII, edited by Jesper Glückstad, David L. Andrews,
Enrique J. Galvez, Proc. of SPIE Vol. 10935, 109350B · © 2019 SPIE
CCC code: 0277-786X/19/$18 · doi: 10.1117/12.2505844

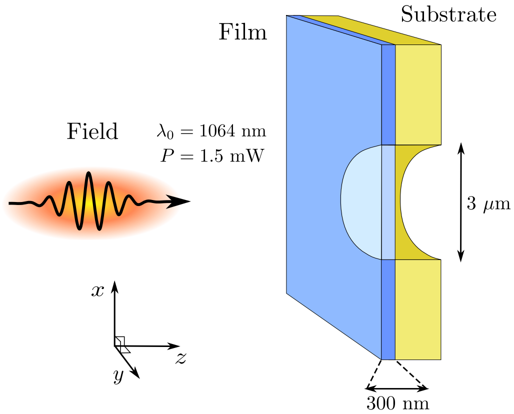

Figure 1. Schematic illustration of light incident to an edge-supported free-standing thin film deposited on top of a substrate. There is a circular microhole in the substrate at the position where light is focused. We assume that there is an atomic bonding between the thin film and the rigid substrate. In the simulations, we use a light beam with a vacuum wavelength $\lambda_0 = 1064$ nm and power $P = 1.5$ mW. The transverse dimensions of the light beam at the position of the film (characterized by the waist radius of 1 μm) are assumed to be smaller than diameter of the microhole so that we do not need to account for the diffraction of light at the edges of the microhole. In the figure, the structure has been split at the position of the microhole to reveal the details. The thickness of the film is 300 nm and the diameter of the hole in the substrate is 3 μm. The atoms of the film are displaced from their initial equilibrium positions by the optical force density. This in turn induces an elastic force density, which redistributes the atomic displacements.

thin film and to relating the measurements to the properties of incoming light. A schematic illustration of light incident on an edge-supported free-standing thin film structure is presented in Fig. 1. In the simulations, we use field intensities well below the irradiation damage threshold of the studied thin film materials so that the observed bending of the thin film is elastic and the use of the elastic force density in the OCD model is justified.

2. OPTOELASTIC CONTINUUM DYNAMICS

2.1 Optical and elastic forces and Newton's equation of motion

In the MP theory of light, the dynamics of the field and the matter are coupled through Newton's equation of motion. In the initial rest frame of the medium, Newton's equation of motion for the mass density of the medium $\rho_{\mathrm{a}}(\mathbf{r},t)$ and the instantaneous position- and time-dependent atomic displacement field $\mathbf{r}_{\mathrm{a}}(\mathbf{r},t)$ is written as[17]

$$\rho_{\mathrm{a}}(\mathbf{r},t)\frac{d^2\mathbf{r}_{\mathrm{a}}(\mathbf{r},t)}{dt^2} = \mathbf{f}_{\mathrm{opt}}(\mathbf{r},t) + \mathbf{f}_{\mathrm{el}}(\mathbf{r},t). \tag{1}$$

Here $\mathbf{f}_{\mathrm{opt}}(\mathbf{r},t)$ is the optical force density experienced by the medium atoms, and $\mathbf{f}_{\mathrm{el}}(\mathbf{r},t)$ is the elastic force density that arises between atoms, which are displaced from their original equilibrium positions by the optical force density. The well-known elastic force density for anisotropic cubic crystals, such as silicon, and for hexagonal crystals, such as graphite, are given in Ref.[22]

The optical force density in the MP theory of light in a lossless dispersive dielectric is presented in Ref.[18] In this work, we use a more general form of the optical force density that can also be applied to lossy nonmagnetic media. This optical force density is given by

$$\mathbf{f}_{\mathrm{opt}} = \underbrace{\rho_{\mathrm{e}}\mathbf{E} + \mu_0\mathbf{J}\times\mathbf{H}}_{\mathbf{f}_{\mathrm{L}}}\underbrace{-\varepsilon_0 n_{\mathrm{g}}\mathbf{E}^2\nabla n_{\mathrm{p}}}_{\mathbf{f}_{\mathrm{int}}}\underbrace{+\frac{n_{\mathrm{p}}n_{\mathrm{g}}-1}{c^2}\frac{\partial}{\partial t}\mathbf{E}\times\mathbf{H}}_{\mathbf{f}_{\mathrm{A}}}. \tag{2}$$

Here ρ_{e} is the density of free electric charges in the medium, n_{p} is the pase refractive index, n_{g} is the group refractive index, $\sigma = \varepsilon_{\mathrm{i}}\omega$ is the electrical conductivity, where ε_{i} is the imaginary part of the permittivity, and $\mathbf{J} = \sigma\mathbf{E}$ is the light-induced current density. The term $\mathbf{f}_{\mathrm{L}}$ in Eq. (2) is the Lorentz force, which leads to damping of the field inside lossy media, $\mathbf{f}_{\mathrm{int}}$ is the interface force, which is related to the changes in the refractive index, and $\mathbf{f}_{\mathrm{A}}$ is the Abraham force, which drives forwards the atomic MDW in the medium as shown in Refs.[17–19,21]

2.2 Momentum and angular momentum of the coupled mass-polariton state of light

The total momentum of the coupled MP state of light is shared between the electromagnetic field and the atomic MDW. This total momentum of the MP and its field and the medium contributions are given by classical integral expressions as

$$\mathbf{p}_{\rm MP} = \int \Big(\frac{\mathbf{E}\times\mathbf{H}}{c^2} + \rho_{\rm a}\mathbf{v}_{\rm a}\Big) d^3r, \tag{3}$$

$$\mathbf{p}_{\rm field} = \int \frac{\mathbf{E}\times\mathbf{H}}{c^2} d^3r, \qquad \mathbf{p}_{\rm MDW} = \int \rho_{\rm a}\mathbf{v}_{\rm a} d^3r. \tag{4}$$

Correspondingly, the total angular momentum of light and its field and the MDW contributions are given by integrals of the well-known expressions of the angular momentum densities of the field and the medium as

$$\mathbf{J}_{\rm MP} = \int \mathbf{r}\times\Big(\frac{\mathbf{E}\times\mathbf{H}}{c^2} + \rho_{\rm a}\mathbf{v}_{\rm a}\Big) d^3r, \tag{5}$$

$$\mathbf{J}_{\rm field} = \int \mathbf{r}\times\Big(\frac{\mathbf{E}\times\mathbf{H}}{c^2}\Big) d^3r, \qquad \mathbf{J}_{\rm MDW} = \int \mathbf{r}\times\rho_{\rm a}\mathbf{v}_{\rm a} d^3r. \tag{6}$$

From Eqs. (3)–(6), it follows that, in the case of a homogeneous medium, the sharing of the angular momentum between the field and the MDW takes place in such a way that the ratio of the angular momenta of the field and the MDW is equal to the ratio of the corresponding linear momenta.

2.3 Momentum conservation at the front surface of the film

In the MP theory of light, the different terms of the optical force density are unambiguously related to the momenta of the incident, reflected, and transmitted fields and the MDW. The conservation law of momentum can be written at the front interface of the film, through which light enters the film from left in Fig. 1, as

$$\mathbf{p}_{\rm field,0} = \mathbf{p}_{\rm field,r} + \mathbf{p}_{\rm field,t} + \mathbf{p}_{\rm MDW} + \mathbf{p}_{\rm int}, \tag{7}$$

where $\mathbf{p}_{\rm field,0}$ is the momentum of the incident light pulse, $\mathbf{p}_{\rm field,r}$ is the momentum of the reflected field, $\mathbf{p}_{\rm field,t}$ is the momentum of the field transmitted inside the film, $\mathbf{p}_{\rm MDW}$ is the momentum of the MDW driven by the Abraham force of the field inside the film, and $\mathbf{p}_{\rm int}$ is the recoil momentum taken by a thin interface layer. These momentum components are given in terms of the different components of the optical force density and the momentum of the incident field in vacuum as

$$\mathbf{p}_{\rm field,r} = -R\mathbf{p}_{\rm field,0}, \tag{8}$$

$$\mathbf{p}_{\rm field,t} = T\frac{\mathbf{p}_{\rm field,0}}{n_{\rm g}}, \tag{9}$$

$$\mathbf{p}_{\rm MDW} = \int\int_{-\infty}^{t} \mathbf{f}_{\rm A} dt' d^3r = T\Big(n_{\rm p} - \frac{1}{n_{\rm g}}\Big)\mathbf{p}_{\rm field,0}, \tag{10}$$

$$\mathbf{p}_{\rm int} = \int\int_{-\infty}^{t} \mathbf{f}_{\rm int} dt' d^3r = (1 + R - n_{\rm p}T)\mathbf{p}_{\rm field,0}. \tag{11}$$

Here, R and T are the conventional power reflection and transmission coefficients of the front interface between the vacuum and the film. Assuming a cw light beam, these coefficients account for the multiple reflections between the two interfaces of the film. Therefore, these coefficients neglect the field transient at the leading edge of the light beam, during which multiple reflections have not yet taken place.

2.4 Momentum conservation in the damping of the field inside the film

Inside the lossy film, the momenta of the field and the MDW that propagate after the first interface of the film are damped by the Lorentz force density. Assuming that the fields are fully damped in the film, the momentum conservation law for the damping can be written as

$$\mathbf{p}_{\rm field,t} + \mathbf{p}_{\rm MDW} = \int\int_{-\infty}^{t} \mathbf{f}_{\rm L} dt' d^3r = n_{\rm p}T\mathbf{p}_{\rm field,0}. \tag{12}$$

The damping of the field and the MDW is exponential and the attenuation coefficient is $\alpha = 2n_{\mathrm{i}}k_0$, where $k_0 = \omega/c$ is the wavenumber of light in vacuum, and n_{i} is the imaginary part of the refractive index. Generalizing Eq. (12) for the case when the field is not fully damped in the film is straightforward by adding damped field and MDW momenta on the right hand side of this equation. These momenta are then incident to the second interface of the film. In this case, the momentum conservation law can be written in the same way as in Eq. (7) with an additional incident MDW momentum on the left hand side, reflected MDW momentum on the right hand side, and no transmitted MDW momentum on the right hand side as there are no atoms in vacuum.

3. SIMULATIONS

Next, we use the OCD model to simulate the propagation of selected LG mode beams in lossy and low-loss dielectric films. As a lossy film material, we use graphite and, as a low-loss film material, we use silicon. Due to the heating effect in the lossy graphite, which is not included in the present simulations, we use a relatively low laser power of 1.5 mW, which is focused on the film surface in an area with a radius that is of the order of 1 μm. The assumed vacuum wavelength of the light beam is $\lambda_0 = 1064$ nm, which is the main wavelength of a conventional Nd:YAG laser. For this wavelength, the phase refractive index of silicon is $n_{\mathrm{Si,p}} = 3.555 + 8.260 \times 10^{-5}i$ and the group refractive index is $n_{\mathrm{Si,g}} = 3.874$.[23] The phase refractive index of graphite is $n_{\mathrm{G,p}} = 3.248 + 2.035i$ and the group refractive index is $n_{\mathrm{G,g}} = 2.429$.[24]

In the simulations, we use a perturbative approach in which we assume, on the basis of previous simulations,[17,19,21] that the back action of the atomic displacements on the field is extremely small and can be neglected. Consequently, we solve the electric and magnetic fields of the cw field by using standard Maxwell's equations. These fields are then used as an input for the OCD model to describe the coupled field-medium dynamics. By using cw field modes as the input for the OCD model, we also neglect the very short field transient at the leading edge of the beam, during which the multiple reflections between the interfaces of the film have not yet taken place. In the present simulations, we assume that the circular edge of the thin film in Fig. 1 is fixed, i.e., the thin film is atomically bonded to the rigid substrate. However, this is not a limitation of the OCD model that could also account for the larger geometry including both the film and the substrate with its true elastic properties.

In the OCD simulations, we use the well-documented elastic properties of the materials. Silicon, which is used as an example of a low-loss thin film material, has an anisotropic cubic lattice structure whose elastic constants in the direction of the (100) plane are $C_{11} = 165.7$ GPa, $C_{12} = 63.9$ GPa, and $C_{44} = 79.6$ GPa.[25] These elastic constants correspond to the bulk modulus of $B = (C_{11} + 2C_{12})/3 = 97.8$ GPa and the shear modulus of $G = C_{44} = 79.6$ GPa. The mass density of silicon is $\rho_{\mathrm{Si}} = 2329$ kg/m^3.[26] Graphite, which has been chosen as a lossy film material, has a hexagonal lattice structure. The five independent elastic constants in the direction of the (100) plane for single-crystalline graphite are $C_{11} = 1109$ GPa, $C_{12} = 139$ GPa, $C_{13} = 0$ GPa, $C_{33} = 38.7$ GPa, and $C_{44} = 4.95$ GPa.[27] The corresponding Reuss averages of the bulk and shear moduli are $B = 36.4$ GPa and $G = 11.3$ GPa. The mass density of graphite is $\rho_{\mathrm{G}} = 2260$ kg/m^3.[27]

3.1 Transmission, reflection, and damping of fields in silicon and graphite films

First, we investigate the transmission, reflection, and damping of the optical field inside the film. Figure 2(a) shows the instantaneous Poynting vector of a left-incoming linearly polarized $\mathrm{LG}_{0,0}$ mode cw field in the low-loss silicon film geometry as a function of the position. The film is located between $z = 0$ and $z = 300$ nm. One can see that the harmonic oscillations of the field are denser and their magnitude is larger inside the silicon film than in vacuum due to the large refractive index of silicon. In the present low-loss case, the field is not damped in the film since the absorption losses are negligible, and it continues to propagate to the right after the film. The amplitude of the field after the film on the right is only slightly smaller than the amplitude before the film on the left as the reflectivity of the film that is thin compared to the wavelength is very small. The total power reflection coefficient of the film is $R = 5.83 \times 10^{-4}$.

Figure 2(b) presents the instantaneous Poynting vector of a left-incoming cw field in the lossy graphite film geometry as a function of the position. Compared to the low-loss case in Fig. 2(a), the oscillations of the Poynting vector on the right extend to essentially negative values, which indicates that power transfer of the reflected field to the left exceeds the power transfer of the incident field to the right. This is related to the total power reflection

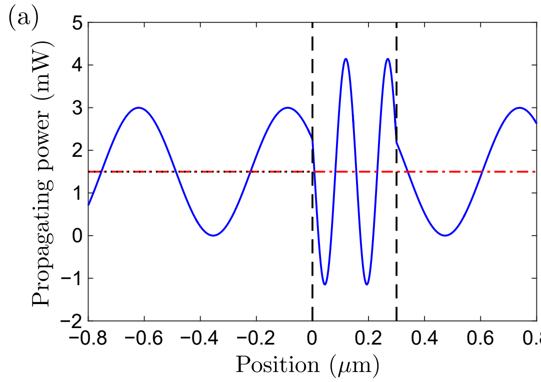

Figure 2. Propagating power of a linearly polarized $LG_{0,0}$ mode laser field, i.e., the integral of the Poynting vector over the transverse plane, (a) for a low-loss silicon film and (b) for a lossy graphite film. The solid line shows the instantaneous propagating power, which is the difference of the right and left propagating powers, the dash-dotted line shows the propagating power averaged over the harmonic cycle, and the dotted line shows the time-averaged incident power 1.5 mW propagating to the right. The vertical dashed lines show the boundaries of the film, which has a thickness of $d = 300$ nm. The field is rapidly attenuated inside the graphite film due to losses related to conductivity while attenuation is very small inside the silicon film. The wavelength of the field is $\lambda_0 = 1064$ nm.

coefficient of the film $R = 0.414$, which is substantially larger than the power reflection coefficient in the low-loss case above. Inside the film in Fig. 2(b), the field is significantly damped due to the absorption losses and there is essentially no field component propagating to the right after the film.

3.2 Atomic displacements due to optical and elastic forces in a low-loss silicon film

Next, we investigate the atomic displacements resulting from the optical and elastic forces. First, we study the case of a low-loss silicon film. We assume a circularly polarized $LG_{0,0}$ mode beam. Figure 3(a) shows the longitudinal atomic displacements along z axis in the plane $y = 0$ μm at $t = 3$ ps after the light beam has been switched on. The dominant contributions of the atomic displacements at the two interfaces near $z = 0$ and $z = 300$ nm result from the optical interface forces described by the second term of Eq. (2). These forces are directed outwards from the film. Note that the total reflectivity of the silicon film is negligible as described in Sec. 3.1. The third term of the optical force density in Eq. (2) results in a forwards shift of atoms inside the film with the atomic MDW associated with light. This contribution is a few orders of magnitude smaller than the atomic displacements at the interfaces. Therefore, this effect is not visible in the scale of Fig. 3(a). The effect of the Lorentz force in the first term of Eq. (2), which is related to the optical losses, is also negligible in the present case due to the very small imaginary part of the refractive index.

Figure 3(b) presents the longitudinal atomic displacements at $t = 35$ ps. One can see that the atomic displacements originating from the interface forces have propagated deeper inside the silicon film. At this instance of time, the magnitudes of the interface displacements have obtained local temporal maxima, i.e., the atomic displacement near the left interface is the smallest and the atomic displacement near the right interface is the largest. When the simulation is continued, the magnitudes of the atomic displacements start to become smaller as the atomic displacement waves starting from the left and right interfaces cancel each other. The local minimum values of the magnitudes of the atomic displacements are obtained at $t = 70$ ps (not shown). After this, the magnitudes of the atomic displacements increase again. The second maximum of the atomic displacements is obtained at $t = 105$ ps, which is presented in Fig. 3(c). The magnitudes of the atomic displacements in this figure are very close to those in Fig. 3(b).

Figures 3(d), 3(e), and 3(f) depict the transverse components of the atomic displacements in the middle of the silicon film at $z = 150$ nm at $t = 3$, $t = 35$, and $t = 105$ ps, respectively. In Fig. 3(d), the atomic displacements in the middle of the film follow purely from the atomic MDW effect and the momentum transfer related to optical absorption. The atomic displacements related to the optical interface forces have not had time to propagate to the middle part of the film in this short time scale since they are mediated deeper in the film by elastic forces at

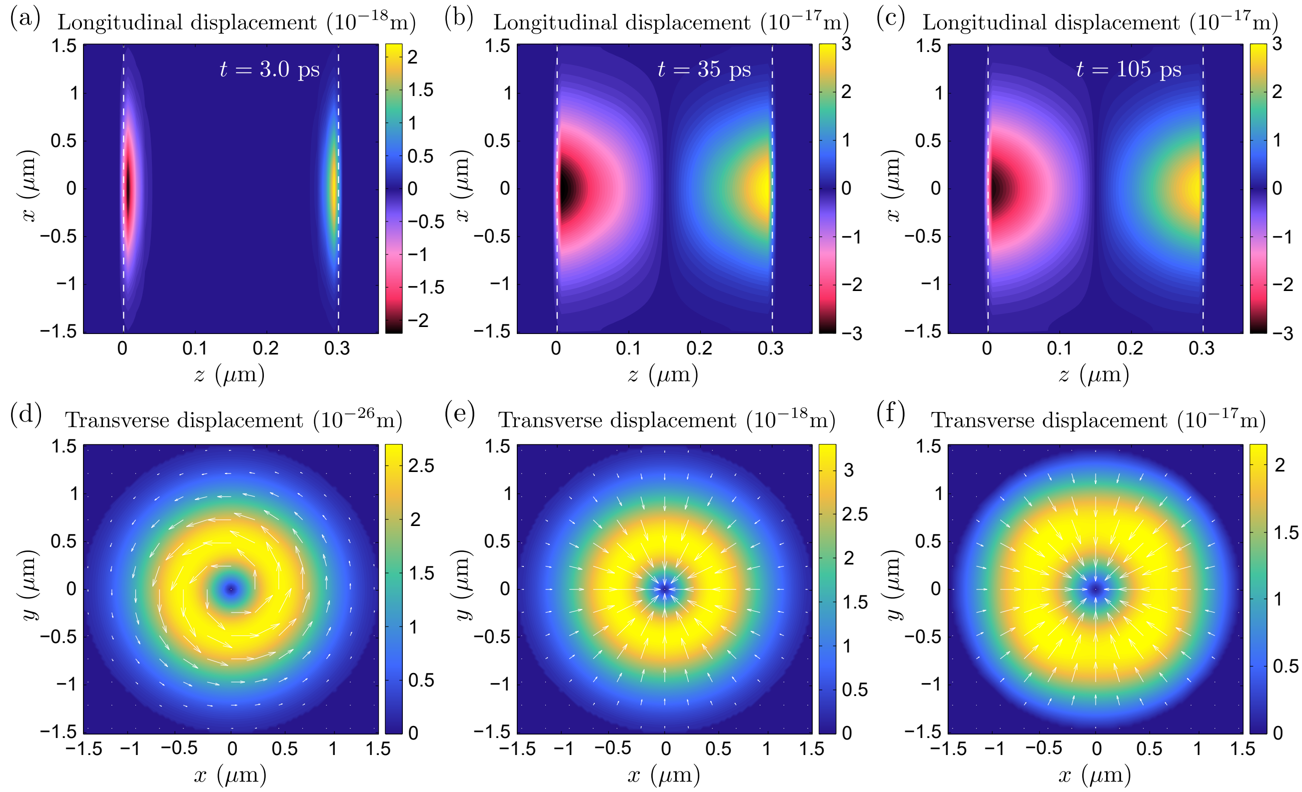

Figure 3. The formation of atomic displacements in the low-loss silicon film at the picosecond time scale due to a circularly polarized $\mathrm{LG}_{0,0}$ mode. (a) At $t = 3$ ps, thin interface layers on both sides of the film have recoiled out of the interfaces due to the optical interface forces. (b) At $t = 35$ ps, the interface displacements have propagated deeper inside the film and their magnitudes have obtained the first temporal local maxima, which depend both on the optical force density and elastic forces between atoms. (c) At $t = 105$ ps, the magnitudes of the interface displacements have obtained the second temporal local maxima. Between the temporal local maxima at $t = 70$ ps, the magnitude of the atomic displacement reaches its minimum values, which are close to zero in the same scale (not shown). The vertical dashed lines show the boundaries of the film, which has a thickness of $d = 300$ nm. The transverse components of the atomic displacements in the middle of the silicon film at $z = 150$ nm are depicted (d) at $t = 3$ ps, (e) at $t = 35$ ps, and (f) at $t = 105$ ps. The wavelength of the field is $\lambda_0 = 1064$ nm and the power is $P = 1.5$ mW.

the velocity of sound, which is vastly smaller in comparison with the velocity of light in the medium. Due to the angular momentum transfer of the circularly polarized $\mathrm{LG}_{0,0}$ mode, the atomic displacements spiral around the optical axis in Fig. 3(d). This follows from the fact that the atomic MDW associated with light carries a major part of the total angular momentum of light in silicon. In Fig. 3(e), the effect of the displacement of atoms at the interfaces have had time to reach the middle part of the film. This results in radial atomic displacements towards the optical axis. This is as expected for the atomic displacements resulting from the elastic stretching of the film in the longitudinal direction by the optical interface forces. The azimuthal atomic displacements related to the angular momentum transfer of the MDW are also present in Fig. 3(e), but they are not visible in the scale of this figure since their magnitude is a few orders smaller than the magnitude of the radial atomic displacements due to the elastic stretching described above.

3.3 Atomic displacements due to optical and elastic forces in a lossy graphite film

Next, we study the atomic displacements resulting from the optical and elastic forces in a lossy graphite film. We assume the same linearly polarized $\mathrm{LG}_{0,0}$ mode beam as in the low-loss case above. Figure 4(a) shows the longitudinal atomic displacements along z axis in the plane $y = 0$ μm at $t = 3$ ps in the case of the lossy graphite film. In contrast to the case of the low-loss silicon film in Fig. 3, the atomic displacements in the present case are dominated by the Lorentz force related to the optical absorption. Therefore, the atomic displacement at the

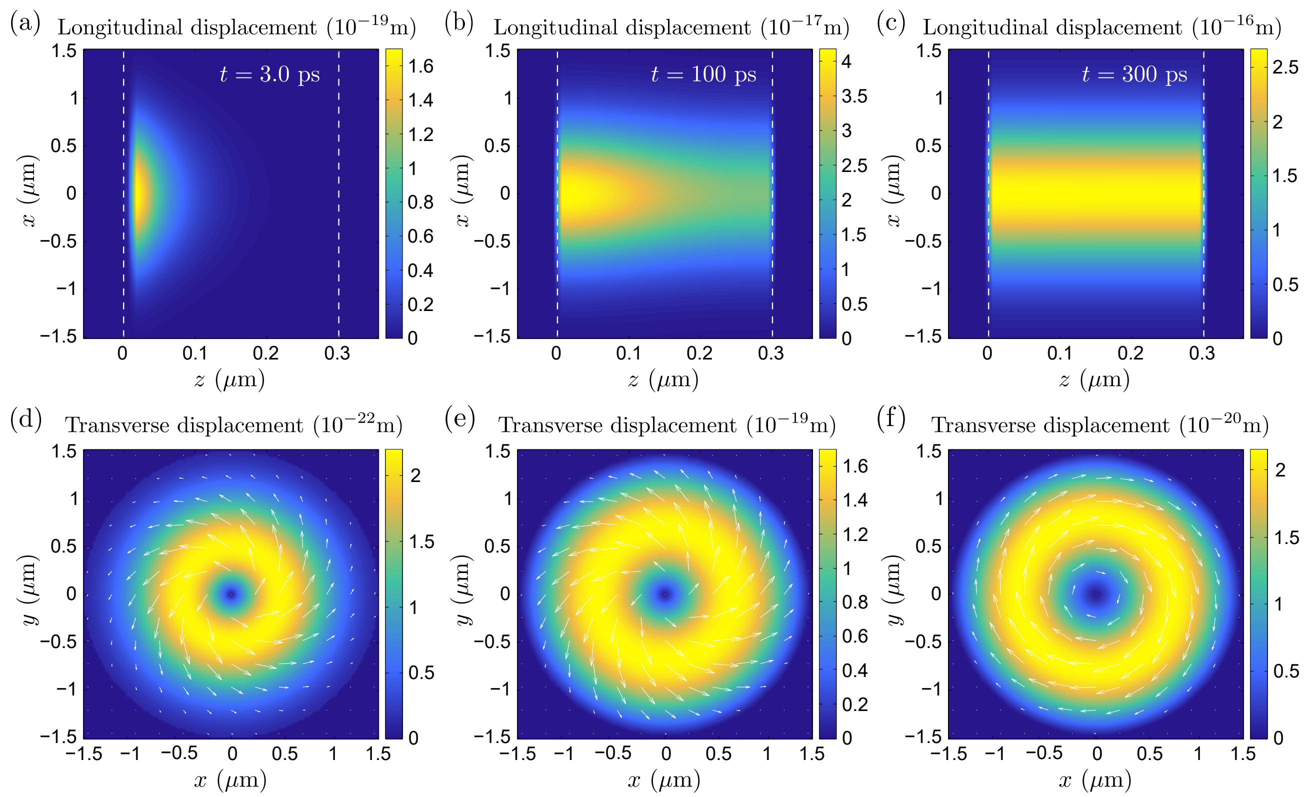

Figure 4. The formation of atomic displacements in the lossy graphite film in the picosecond time scale due to a circularly polarized $\mathrm{LG}_{0,0}$ mode. (a) At $t = 3$ ps, a thin layer of the front interface has recoiled backwards due to the optical interface force and the atoms inside the medium near the front interface have recoiled forwards due to the optical Lorentz force related to absorption losses. The total atomic displacement is determined by both effects, but the absorption related effect dominates. (b) At $t = 100$ ps, the atoms are displaced forwards also deeper inside the graphite film. The optical Lorentz force inside the film dominates the interface forces. (c) At $t = 300$ ps, the atomic displacement inside the film has reached values that are approximately constant in the z direction. The vertical dashed lines show the boundaries of the film, which has a thickness of $d = 300$ nm. The transverse components of the atomic displacements in the middle of the graphite film at $z = 150$ nm are depicted (d) at $t = 3$ ps, (e) at $t = 100$ ps, and (f) at $t = 300$ ps. The wavelength of the field is $\lambda_0 = 1064$ nm and the power is $P = 1.5$ mW.

first interface of the film is directed inside the film in Fig. 4(a). The interface force at the second interface of the film is negligible since the fields are fully damped inside the film as shown in Fig. 2(b).

Figure 4(b) shows the longitudinal atomic displacements in the graphite film at $t = 35$ ps. One can observe that the atomic displacements following from the momentum transfer due to the reflection and absorption near the first interface have propagated deeper inside the graphite film. Part of the absorption takes place deep inside the film where the field has not yet damped to zero. Therefore, the propagation of the atomic displacements from the first interface to deeper in the film is not fully governed by the elastic forces in contrast to the propagation of the atomic displacements following from the pure optical interface forces in Fig. 3. In Fig. 4(c), the atomic displacements are depicted at $t = 300$ ps. At this instance of time, the atomic displacement inside the film has reached values that are approximately constant in the z direction. These constant values, however, continue to develop as a function of time.

Figures 4(d), 4(e), and 4(f) present the transverse components of the atomic displacements in the middle of the graphite film at $z = 150$ nm at $t = 3$, $t = 100$, and $t = 300$ ps, respectively. In Fig. 4(d), the atomic displacements in the middle of the film follow from both the atomic MDW effect and the momentum transfer related to optical absorption. The optical absorption is the dominating factor in the present case. This is related to the larger magnitude of the transverse component of the atomic displacements in Fig. 4(d) in comparison to those in Fig. 3(d). Due to the absorption of angular momentum related to the circularly polarized $LG_{0,0}$ mode, the atomic displacements spiral around the optical axis in Fig. 4(d) and in Figs. 4(e) and 4(f), where the atomic displacement is depicted at later times. Also, one can see that the radial component of the atomic displacements is directed outwards from the optical axis in Figs. 4(e) and 4(f) in contrast to the inwards-directed radial component of the atomic displacements in the low-loss case in Figs. 3(e) and 3(f). This is related to the fact that, in the low-loss case, the film has been stretched by the optical interface forces, while in the present lossy case, the film is pushed starting from the first interface by the optical force related to absorption. The resulting elastic displacements of atoms inside the film are consequently opposite. That the azimuthal atomic displacements change sign between Figs. 4(e) and 4(f) follows from the elastic recoil effect.

3.4 Force and torque at the edge of the thin film

Since the thin film studied in the present work is supported at its edge, there is an effective external force that keeps the edge of the film fixed to its original position. By the law of action and counteraction, this force is equal in magnitude and opposite in direction to the force that the atoms at the edge of the film experience due to the elastic bending of the film. Therefore, we can use the OCD simulations to calculate the total external force experienced by the thin film through its edge. Regarding the conservation law of the total momentum, this external force is of fundamental importance since, due to the fixed edge of the film, the system of the film and the electromagnetic field cannot be considered to be closed.

Figure 5(a) presents the time dependence of the total force experienced by the edge atoms of the low-loss silicon film due to the bending of the film. As expected, this force varies between temporal minima and maxima in the course of time. The period of this elastic oscillation is determined by the elastic constants of the silicon

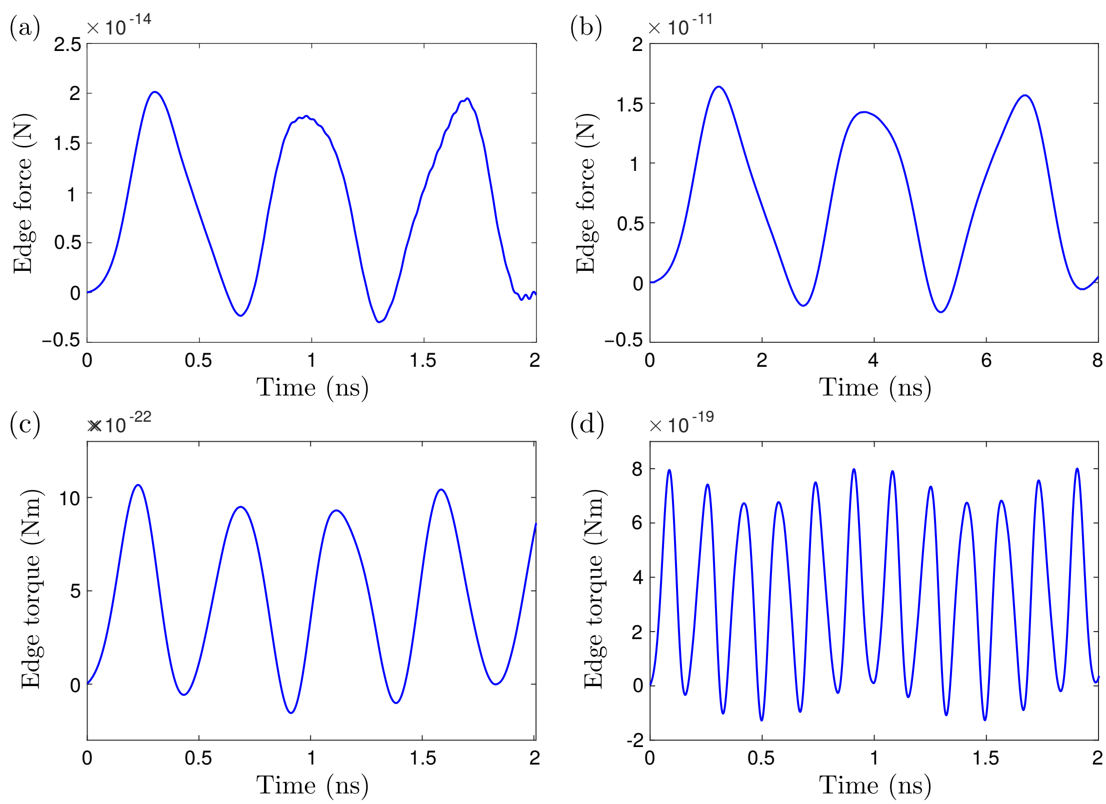

Figure 5. Time dependence of the total force experienced by the structure supporting (a) the low-loss silicon film and (b) the lossy graphite film through its edge. Positive values indicate force to the right in Fig. 1. By the law of action and counteraction, this edge force is equal in magnitude and opposite in direction to the force that the thin film experiences due to the structure supporting it through the edge. The edge torques for the low-loss silicon film and the lossy graphite film are shown in panels (c) and (d). The wavelength of the field is $\lambda_0 = 1064$ nm and the power is $P = 1.5$ mW.

film. The corresponding force and the related elastic oscillation in the case of the lossy graphite film is shown in Fig. 5(b). Note that the forms of the graphs in Figs. 5(a) and 5(b) are identical. However, the magnitude of the force and the time scale of its oscillation are larger in the case of the graphite film. The larger magnitude follows from the larger momentum transfer with the electromagnetic field due to the absorption losses. The larger time scale of the oscillation of the edge force follows from the smaller elastic constants in the direction perpendicular to the graphene layers forming the graphite film.

Figures 5(c) and 5(d) show the time dependence of the total torques experienced by the edges of the silicon and graphite films, respectively. The total edge torques are seen to oscillate as a function of time as expected. The period of these oscillations are determined by the elastic constants in the transverse direction of the film. In particular, note that the period of the oscillation of the torque is shorter in the case of the graphite film than in the case of the silicon film due to the large elastic constants of graphite along the graphene layers in its structure. Thus, our simulation results are in good agreement with our understanding of the expected elastic behavior of the silicon and graphite films based on their molecular structure.

4. CONCLUSIONS

In conclusion, we have used the OCD model to simulate the dynamics of medium atoms in lossy and low-loss thin film structures. Our results show how the different force components related to reflection, transmission, absorption, and the atomic MDW bend and twist the film. We have also investigated the time dependence of the total forces and torques that are exerted to the structure supporting the thin film through its edge. The simulations also aim at finding possible experimental setups for the studies of the coupled dynamics of light and the thin film atoms and to relating the measurements to the properties of incoming light. The results also indicate that thin film structures may not be optimal for the direct experimental verification of the atomic MDW effect since it is hidden under other effects. The OCD model allows detailed simulations of the optoelastic dynamics in any material geometry under the influence of the optical force field. For instance, one can model the coupled field-medium dynamics in thin films for possible device development needs. The OCD simulations can also be used for the optimization of possible setups that can be planned for the experimental verification of the atomic MDW associated with light.

ACKNOWLEDGMENTS

This work has been funded in part by the Academy of Finland under Contracts No. 287074 and No. 318197.

REFERENCES

[1] K. Y. Bliokh and A. Aiello, "Goos-Hänchen and Imbert-Fedorov beam shifts: an overview," *J. Opt.* **15**, 014001 (2013).

[2] K. Y. Bliokh, J. Dressel, and F. Nori, "Conservation of the spin and orbital angular momenta in electromagnetism," *New J. Phys.* **16**, 093037 (2014).

[3] K. Y. Bliokh, F. J. Rodríguez-Fortuño, F. Nori, and A. V. Zayats, "Spin-orbit interactions of light," *Nat. Photon.* **9**, 796 (2015).

[4] L. Du, Z. Man, Y. Zhang, C. Min, S. Zhu, and X. Yuan, "Manipulating orbital angular momentum of light with tailored in-plane polarization states," *Sci. Rep.* **7**, 41001 (2017).

[5] F. Alpeggiani, K. Y. Bliokh, F. Nori, and L. Kuipers, "Electromagnetic helicity in complex media," *Phys. Rev. Lett.* **120**, 243605 (2018).

[6] A. Y. Bekshaev, K. Y. Bliokh, and F. Nori, "Transverse spin and momentum in two-wave interference," *Phys. Rev. X* **5**, 011039 (2015).

[7] J. Lin, J. P. B. Mueller, Q. Wang, G. Yuan, N. Antoniou, X.-C. Yuan, and F. Capasso, "Polarization-controlled tunable directional coupling of surface plasmon polaritons," *Science* **340**, 331 (2013).

[8] K. Y. Bliokh, A. Y. Bekshaev, and F. Nori, "Optical momentum, spin, and angular momentum in dispersive media," *Phys. Rev. Lett.* **119**, 073901 (2017).

[9] K. Y. Bliokh, A. Y. Bekshaev, and F. Nori, "Optical momentum and angular momentum in complex media: from the Abraham-Minkowski debate to unusual properties of surface plasmon-polaritons," *New J. Phys.* **19**, 123014 (2017).

[10] K. Y. Bliokh, A. Y. Bekshaev, and F. Nori, "Extraordinary momentum and spin in evanescent waves," *Nat. Commun.* **5**, 3300 (2014).

[11] A. Mair, A. Vaziri, G. Weihs, and A. Zeilinger, "Entanglement of the orbital angular momentum states of photons," *Nature* **412**, 313 (2001).

[12] G. Molina-Terriza, J. P. Torres, and L. Torner, "Twisted photons," *Nat. Photon.* **3**, 305 (2007).

[13] T. Požar and J. Možina, "Measurement of elastic waves induced by the reflection of light," *Phys. Rev. Lett.* **111**, 185501 (2013).

[14] T. Požar, J. Laloš, A. Babnik, R. Petkovšek, M. Bethune-Waddell, K. J. Chau, G. V. B. Lukasievicz, and N. G. C. Astrath, "Isolated detection of elastic waves driven by the momentum of light," *Nat. Commun.* **9**, 3340 (2018).

[15] A. Kundu, R. Rani, and K. S. Hazra, "Graphene oxide demonstrates experimental confirmation of Abraham pressure on solid surface," *Sci. Rep.* **7**, 42538 (2017).

[16] I. Brevik, "Analysis of recent interpretations of the Abraham-Minkowski problem," *Phys. Rev. A* **98**, 043847 (2018).

[17] M. Partanen, T. Häyrynen, J. Oksanen, and J. Tulkki, "Photon mass drag and the momentum of light in a medium," *Phys. Rev. A* **95**, 063850 (2017).

[18] M. Partanen and J. Tulkki, "Mass-polariton theory of light in dispersive media," *Phys. Rev. A* **96**, 063834 (2017).

[19] M. Partanen and J. Tulkki, "Mass-polariton theory of sharing the total angular momentum of light between the field and matter," *Phys. Rev. A* **98**, 033813 (2018).

[20] M. Partanen and J. Tulkki, "Lorentz covariance of the mass-polariton theory of light," arXiv:1811.09456 (2018).

[21] M. Partanen and J. Tulkki, "Light-driven mass density wave dynamics in optical fibers," *Opt. Express* **26**, 22046 (2018).

[22] C. Kittel, *Introduction to Solid State Physics*, Wiley, Hoboken, NJ (2005).

[23] C. Schinke, P. C. Peest, J. Schmidt, R. Brendel, K. Bothe, M. R. Vogt, I. Kröger, S. Winter, A. Schirmacher, S. Lim, H. T. Nguyen, and D. MacDonald, "Uncertainty analysis for the coefficient of band-to-band absorption of crystalline silicon," *AIP Advances* **5**, 067168 (2015).

[24] A. B. Djurišić and E. H. Li, "Optical properties of graphite," *J. Appl. Phys.* **85**, 7404 (1999).

[25] M. A. Hopcroft, W. D. Nix, and T. W. Kenny, "What is the Young's modulus of silicon?" *J. Microelectromech. Syst.* **19**, 229 (2010).

[26] D. R. Lide, ed., *CRC Handbook of Chemistry and Physics*, CRC Press, Boca Raton, FL (2004).

[27] A. Bosak, M. Krisch, M. Mohr, J. Maultzsch, and C. Thomsen, "Elasticity of single-crystalline graphite: Inelastic x-ray scattering study," *Phys. Rev. B* **75**, 153408 (2007).